Dimensionless numbers

Ar''	mod. Archimedes number (Eq. (7))
K_c''	mod. liquid number (Eq. (6))
Re	Reynolds number ($d_p\ w_{rel}/\ \nu_c$)

References

[1] Schilp, R., Blass, E., *Chem. Eng. Commun. 28* (1984) pp. 85 – 98.
[2] Schilp, R., Blass, E., *Ger. Chem. Eng 8* (1985) pp. 44 – 47.
[3] Otillinger, F., Blass, E., *Preprints ISEC '86*, Munich, Vol. III, 1986, pp. 445 – 452.
[4] Meon, W., Blass, E., *Chem. Eng Technol. 10* (1987) pp. 281 – 289.
[5] Hirschmann, K., *Dissertation*, TU München 1984.
[6] Clift, R., Grace, J.R., Weber, M.E., *Bubbles, Drops and Particles*, Academic Press, New York 1978.
[7] Newman, A.B., *Trans. Am. Inst. Chem. Eng. 27* (1931) pp. 203 – 211.
[8] Kronig, R., Brink, J.C., *Appl. Sci. Res. A. 2* (1951) pp. 142 – 154.
[9] Skelland, A.H.P., Minhas, S.S., *AIChE J. 17* (1971) pp. 1316 – 1324.
[10] Handlos, A.E., Baron, Th., *AIChE J. 3* (1957) pp. 127 – 136.
[11] Pilhofer, Th., Mewes, D., *Siebbodenextraktionskolonnen*, reprotext Verlag Chemie, Weinheim 1979.
[12] Olander, D.R., *AIChE J. 12* (1966) No. 5, pp. 1018 – 1019.
[13] Levich, V.G., *Physiochemical Hydrodynamics*, Prentice Hall 1962.
[14] Higbie, R., *Trans. Am. Inst. Chem. Eng. 31* (1935) pp. 365 – 389.
[15] Plucinski, P., Pajak, M., *Inz. Chem. Proc. 2* (1981) pp. 125 – 137.
[16] Plucinski, P., Pajak, M., *Inz. Chem. Proc. 2* (1981) pp. 139 – 155.
[17] Skelland, A.H.P., Conger, W.L., *Ind. Eng Chem. Process Des. Dev. 62* (1973) No. 4, pp. 448 – 454.
[18] Hu. S., Kintner, R.C., *AIChE J. 31* (1955) No. 1, pp. 42 – 48.
[19] Keith, F.W., Hixson, A.N., *Ind. Eng Chem. 47* (1955) No. 2, pp. 258 – 267.
[20] Klee, A.J., Treybal, R.E., *AIChE J. 2* (1956) No. 4, pp. 444 – 447.
[21] Johnson, A.I., Braida, L., *Can. J. Chem. Eng 35* (1957) No. 12, pp. 165 – 172.
[22] Strom, I.R., Kintner, R.C., *AIChE J. 4* (1958) No. 2, pp. 153 – 156.
[23] Krishna, P.M., Venkateswarlu, D., Narasimhamurty, G.S.R., *J. Chem. Eng Data 4* (1959) No. 4, pp. 336 – 343.
[24] Thorensen, G., Stordalen, R.M., Terjesen, S.G., *Chem. Eng Sci. 23* (1968) pp. 413 – 426.
[25] Mahendru, H.L., Hackl, A., *Chem.-Ing.-Tech. 53* (1981) No. 1, p. 55.

Subcooled Boiling Heat Transfer to R 12 in an Annular Vertical Channel

Holger Bräuer and Franz Mayinger*

Detailed knowledge of the physical phenomena involved in subcooled boiling is of great importance for the design of liquid-cooled heat generating systems with high heat fluxes. Experimental heat transfer data were obtained for forced convective boiling of dichloro-difluoroethane (R 12). The flow is circulated upwards through a concentric annular vertical channel. The inner and outer diameters of the annulus are 0.016 m and 0.03 m respectively. The reduced pressures studied were $0.24 \leq p/p_{crit} \leq 0.8$, inlet subcooling varied from 10 to 75 K and mass fluxes from 500 to 3000 kg/m^{2}s, which corresponds to Re numbers from 30000 to 300000. The experiments, described in this study, demonstrate that liquid fluorocarbons show certain unusual boiling characteristics in the subcooled flow, such as hysteresis of the boiling curve. These characteristics are attributed to the properties of the fluid, mainly the Pr number and the very low surface tension. The pronounced boiling curve hysteresis can be explained by the fact that large nucleation sites may have been flooded prior to incipient boiling. A dimensionless regression formula is presented which predicts the onset of subcooled boiling as a function of reduced pressure (p/p_{crit}), Boiling – (Bo), Reynolds – (Re), and a modified Jacob number (Ja), over the whole range of parameters studied, with a good accuracy, including water data from literature.

1 Introduction

The liquid supplied to flow boiling channels is usually in a subcooled state. In such systems, the first occurring heat transfer process is that of convective heat transfer to single-phase flow in liquid form up to the point "onset of nucleate boiling" (ONB) as shown in Fig. 1, which presents the lower part of the Nukijama curve. This point marks the initiation of nucleate boiling.

The bulk liquid temperature at this point is generally lower than the saturation value. The boiling process up to the point where the bulk of the liquid reaches the saturation temperature is referred to as subcooled boiling. This range can be divided into partial nucleate boiling and fully developed nucleate boiling. Fully

* Dipl.-Ing. H. Bräuer and Prof. Dr.-Ing. F. Mayinger, Lehrstuhl A für Thermodynamik der Technischen Universität München, Arcisstr. 21, D-8000 München 2.

© VCH Verlagsgesellschaft mbH, D-6940 Weinheim, 1988

0930-7516/88/0510-0320 $02.50/0

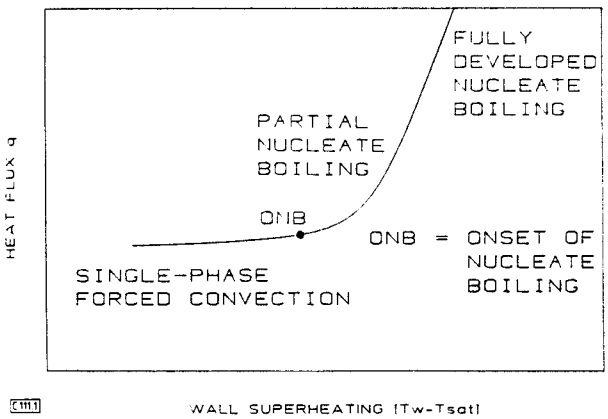

Fig. 1. Transition from single-phase forced convection to fully developed boiling.

developed nucleate boiling is attained when the heat transfer coefficient no longer depends on the mass flux or the degree of subcooling. In this case, the heat transfer coefficient is only a function of the heat flux and of the physical properties of the substance.

In partial nucleate boiling, the heat transfer coefficient does depend on the mass flux and on the degree of subcooling.

These characteristics of subcooled boiling flow have been extensively investigated but most of the available studies were performed with water. For the conditions of incipient boiling with water, Sato and Matsumura [1], Bergles and Rohsenow [2], and Davis and Anderson [3] proposed analytical models based on the existence of cavities on the heated surface. Other investigations dealt with the criteria for the point of net vapour generation and bubble behaviour [4 – 8], but only limited tests have been carried out on other fluids, especially refrigerants. Using R 113, Hino and Ueda [9] and, using R 11, Abdelmessih [10], observed wall superheating which is independent of the mass flux and inlet subcooling. A more detailed literature review can be found in publication [11].

Data for R 12 on nucleation with forced convection and on growth and detachment of bubbles have so far not been available in literature.

2 Experimental Set-up and Test Procedure

The experimental facility, employed in this study, is a closed loop, as shown in Fig. 2. It is designed to operate with R 12, up to the critical pressure.

A centrifugal pump is used to circulate the refrigerant in the loop. The liquid enters the preheater through a controlling valve and an orifice. The preheater uses electrical energy to generate the exact temperature, i.e. the subcooling conditions at the inlet of the test section. From the preheater, the liquid passes through the test section where it is further heated. The resulting two-phase flow then enters the water-cooled condenser and from there flows back to the pump. Other main components of the loop are a filter to rid the flow from particles and a pressurizer,

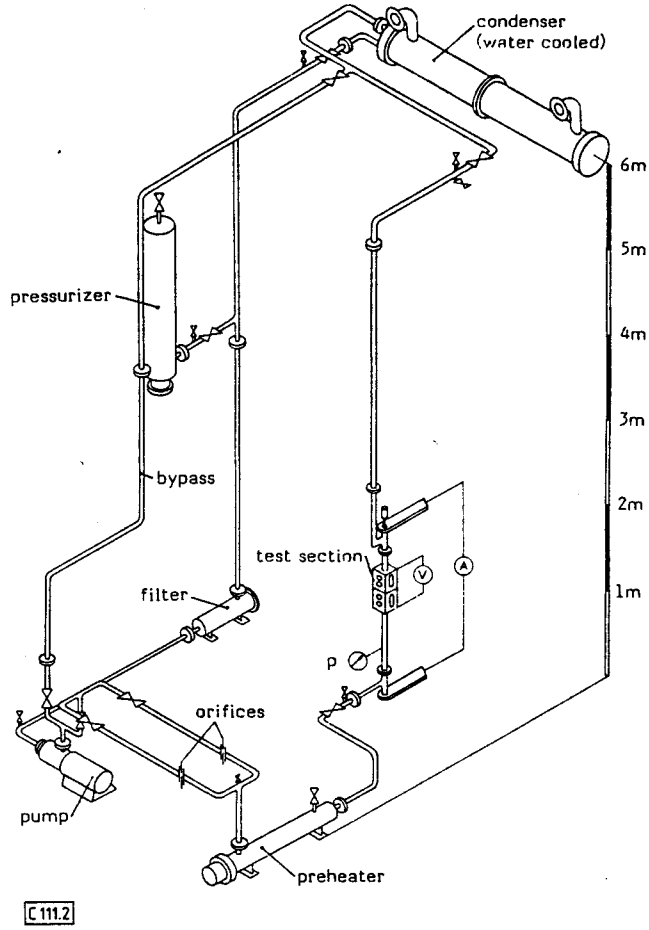

Fig. 2. Test loop.

which ensures constant pressure in the loop during the test runs with the aid of a compressible vapour cushion in its top section. The lower section is filled with R 12 in liquid form, maintained at saturation temperature, corresponding to the desired pressure, by electric heating.

The test section itself, as shown in Fig. 3, is a vertically arranged concentric annulus with the inner tube consisting of three sections of the same diameter, one above the other, namely the unheated entrance region, stainless steel heater, and unheated outlet region.

The inner tube has an outer diameter of 16 mm with wall thickness of 0.5 mm and its heated part is 650 mm long. Heat is supplied at a uniform rate by passing direct electric current through the tube wall. The outer tube is made of a duran glass with inner diameter of 30 mm. The resulting hydraulic diameter of the annulus is 14 mm.

The wall temperatures are measured by 5 shielded Cr-Al thermocouples (diameter of shielding 0.5 mm). These thermocouples are arranged over the length and circumference of the inner tube, as also shown in Fig. 3.

The onset of subcooled boiling is measured during slow heating transient, by recording the signals of the thermocouples in the

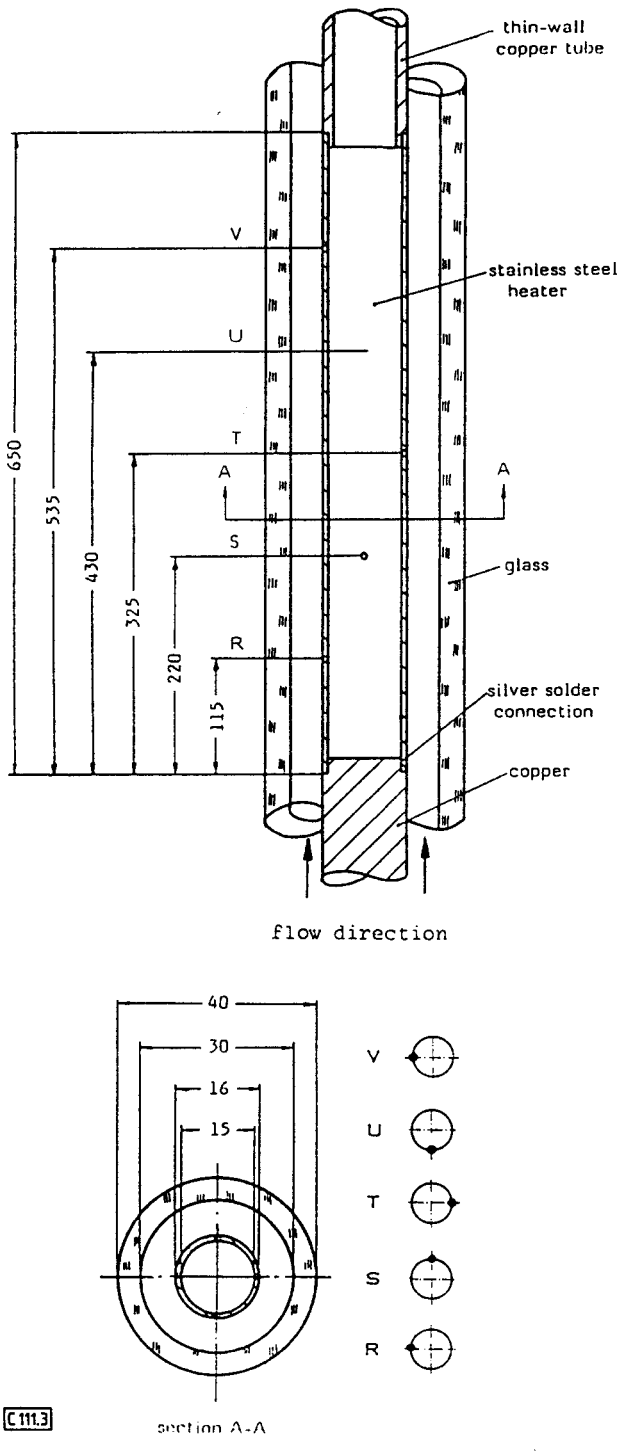

Fig. 3. Test section and arrangement of thermocouples (all dimensions in mm; *R, S, T, U, V* thermocouples).

heated wall. At constant system pressure, mass flow rate and inlet subcooling, the heat flux of the inner tube in the test section increases slowly and linearly with time. The transient is slow enough to guarantee pseudo-steady conditions over the cross-section by heat conduction in the tube wall and turbulent heat transfer in the fluid. In pure single-phase flow, the heat transfer coefficient is a function of flow conditions only, i.e. it is constant during this period of the heating transient. Therefore, the wall temperatures increase linearly with time.

When subcooled boiling starts, the heat transfer coefficient suddenly undergoes a step change, which is observed as a break in the plot of temperature versus time. With R 12, this break is so pronounced that even a stepwise temperature decrease can be seen at the exact moment at which subcooled boiling starts, as demonstrated in Fig. 4, where the wall temperature and heat flux are plotted versus time. With continuing heat supply, the boiling zone expands upstream, downwards and when the signal of the thermocouple "R", see Fig. 3, indicates that the nucleate boiling has reached the entrance region, the maximum heat flux for this particular run has been achieved. In order to check the wall temperature behaviour when boiling is terminated and the heat transfer mode changes from boiling to single-phase convection, the heat flux is temporarily reduced in the same way as described above until boiling is terminated. Obviously, no temperature jump does occur now when subcooled boiling subsides but the wall temperature decreases continuously with decreasing heat flux.

Before discussing the influence of several parameters on nucleate boiling, a few remarks will be made about the single-phase forced convection heat transfer which induces the subcooled boiling.

3 Calculation of Radial Temperature Profiles before the Start of Boiling

In order to obtain more information about the influence of boundary layer conditions and physical properties on the onset of subcooled boiling, the authors considered the boundary layer and applied the conservation laws together with the boundary layer equations from literature. Solving the equation systems numerically, fluid temperature could be calculated at any location in the annular channel, not only in the axial but also in the radial direction.

It is assumed that the annulus is concentric and the flow in it is axisymmetric. Axial and radial coordinates are denoted by x and r respectively. R_i is the inner and R_o the outer radius of the annulus.

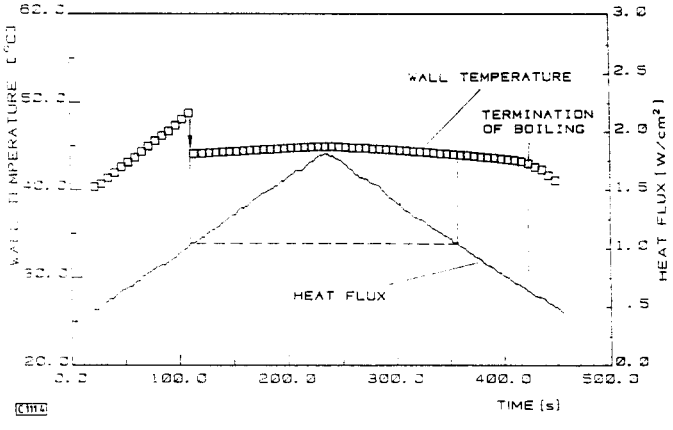

Fig. 4. Wall temperature and heat flux profiles.

Taking into account the radial heat transport and the enthalpy transport in axial direction in the refrigerant, it can be seen that this leads to the following partial differential equation:[1)]

$$-\left(k_{\mathrm{eff}}\, A\, \frac{\partial T(x,r)}{\partial r}\right)_{r} + \left(k_{\mathrm{eff}}\, A\, \frac{\partial T(x,r)}{\partial r}\right)_{r+\Delta r} + \left(\varrho\, c_{\mathrm{p}}\, A\, u\, T(x,r)\right)_{x} - \left(\varrho\, c_{\mathrm{p}}\, A\, u\, T(x,r)\right)_{x+\Delta x} = 0 \quad . \quad (1)$$

In order to describe the effective thermal conductivity k_{eff}, the authors use the eddy viscosity concept in the one-equation model of Norris and Reynolds [12]. This model calculates the turbulent kinetic energy k from the transport equation, taking into account the dissipation and production of turbulent energy.

$$\varrho\, u\, \frac{\partial k}{\partial x}\, r\, \partial r = -\varrho\, \varepsilon\, r\, \partial r + \mu_{\mathrm{t}} \left(\frac{\partial u}{\partial r}\right)^{2} r\, \partial r + \left(\mu_{\mathrm{eff}}\, r\, \frac{\partial k}{\partial r}\right)_{r+\Delta r} - \left(\mu_{\mathrm{eff}}\, r\, \frac{\partial k}{\partial r}\right)_{r} \quad . \quad (2)$$

The velocity profile results from the momentum balance:

$$0 = -\varrho\, u\, 2\, \pi\, r\, \partial r\, \frac{\partial u}{\partial x} - 2\, \pi\, r\, \partial r \left(\frac{\partial p}{\partial x}\right)_{\mathrm{fric}} + \left(\mu_{\mathrm{eff}}\, 2\, \pi\, r\, \frac{\partial u}{\partial r}\right)_{r+\Delta r} - \left(\mu_{\mathrm{eff}}\, 2\, \pi\, r\, \frac{\partial u}{\partial r}\right)_{r} \quad . \quad (3)$$

A fully implicit method with variable physical properties is used to solve the resulting set of equations. The Thomas algorithm was applied to find a solution of the formed tridiagonal matrix.

4 Analysis of Onset of Subcooled Boiling and Associated Heat Transfer

Subcooled boiling heat transfer in an annular vertical channel was investigated systematically at various mass fluxes (m = 500, 1000, 1500, 2000, and 3000 kg/m^{2}s), reduced pressures (p/p_{crit} = 0.242, 0.290, 0.363, 0.484, 0.605, 0.800), heat fluxes (q = 1 to 20 W/cm^2) and liquid subcooling (($T_{\mathrm{sat}} - T_{\mathrm{inlet}}$) = 10, 20, 30, 40, 50, 75 K). The obtained results are discussed in the following chapters.

4.1 The Boiling Hysteresis Phenomenon

During heating, as soon as incipient boiling is initiated, a sharp drop in wall superheating takes place. After this jump, the measured curve is close to that of fully developed boiling. The temperature profile for decreasing heat flux follows that generated by increasing the heat flux until boiling is terminated. From this point, the curve continues to decline smoothly, to merge with the single-phase forced convection curve. This behaviour is traditionally referred to as "hysteresis" and is even more clearly demonstrated in Fig. 5, where the heat flux is plotted against the wall superheating for two different mass flow rates.

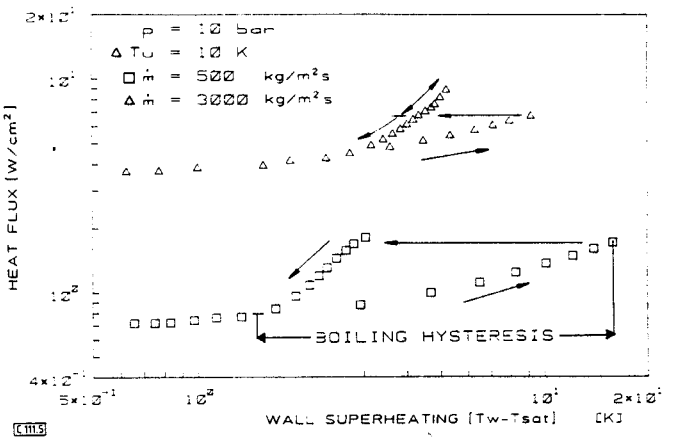

Fig. 5. Boiling curves at different mass fluxes.

For boiling water, this considerable wall superheating has not been reported in literature. To explain this difference, a comparison of some physical properties of water with those of R 12 is shown in Table 1. The basis of comparison was the reduced pressure.

Table 1 shows that the surface tension of water is more than triple that of R 12. Therefore, it can be assumed that, in R 12, the larger cavities on the heated wall will probably be flooded, i.e. wetted and filled with liquid prior to incipient boiling and are, therefore, not available for nucleation. If this is the case, the residual volume in those cavities, which are not flooded, is very small and a correspondingly high superheating ΔT_{ONB} is required to activate these cavities. This may be an explanation of the measured high wall superheating needed for the activation of boiling in R 12, as shown in Fig. 5.

4.2 Influence of Various Parameters on Heat Transfer at the Onset of Subcooled Boiling

The onset of subcooled boiling is influenced by flow velocity, temperature in the boundary layer and physical properties of the fluid. Fig. 6 presents the heat flux, at which subcooled boiling starts, plotted versus the local subcooling of the liquid with the mass flux as parameter. The measurements showed that the heat flux q_{ONB} is scarcely affected by system pressure and, therefore, only the lines for 25 bar are plotted in the diagram,

Table 1. Physical properties of water and refrigerant R 12 at reduced pressure p/p_{crit} in the range $0 \le p/p_{\mathrm{crit}} \le 0.75$, according to [13].

μ_{H_2O}	=	0.466	μ_{R12}	[kg/m s]
k_{H_2O}	=	7.330	k_{R12}	[W/m K]
σ_{H_2O}	=	3.242	σ_{R12}	[N/m]
Δh_{vH_2O}	=	12.14	Δh_{vR12}	[J/kg]
Pr_{H_2O}	=	0.33	Pr_{R12}	[–]

1) List of symbols at the end of the paper.

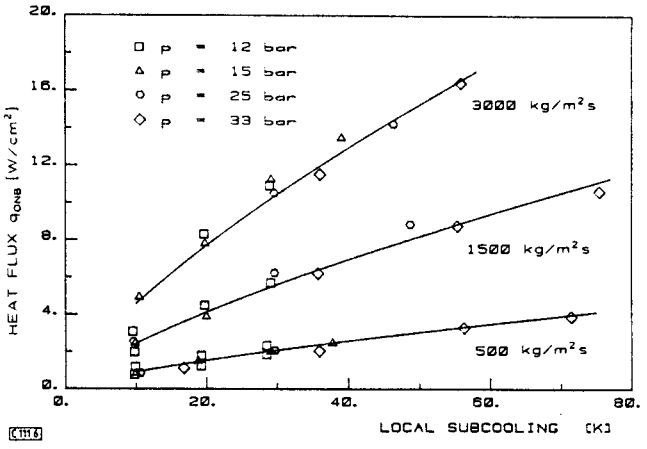

Fig. 6. Onset of nucleation in forced convection subcooled boiling.

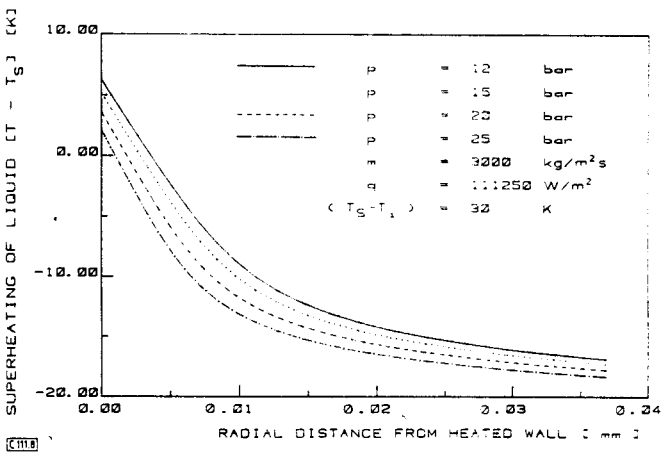

Fig. 8. Radial temperature profiles at a given axial location.

representing the whole range of studied system pressure with a good accuracy.

A better illustration of this slight influence of pressure on heat flux q_{ONB} is given by Fig. 7, which shows a plot of q_{ONB} versus the system pressure for different mass fluxes and local degrees of subcooling.

In an attempt to explain this behaviour, the analytical procedure, briefly described in chapter 3, was used for the calculation of the temperature distribution in the boundary layer prior to boiling. Fig. 8 shows the calculated difference between fluid temperature and saturation temperature at different radial locations plotted versus the distance from heated wall at a given axial location. The curves in the diagram correspond to constant mass flux and constant inlet subcooling but with pressures varying between 12 and 25 bar.

It is obvious that the temperature curves in the diagram are similar. As is well-known from literature, the total amount of energy supplied to the fluid for nucleation is almost independent of system pressure.

With a given pressure, only the absolute temperature exerts an influence on the radial temperature profile of physical properties. The absolute temperature increases with increasing pressure. This results in a decrease of thermal conductivity k and in an increase of the heat capacity c_p of the refrigerant. Both physical properties contribute to a decrease of the gradient of the radial temperature profile and result in a thinner thermal boundary layer.

Starting from the simple equation $p = 2\,\sigma/R$ for the mechanical equilibrium of a spherical vapour nucleus, surrounded by liquid, it can be seen that the excess pressure and thus the superheating in the vapour nucleus is proportional to the surface tension of the refrigerant which also decreases with increasing system pressure.

Hence, it can be concluded that the wall superheating ΔT_{ONB} at incipient boiling must decrease with increasing system pressure. This behaviour is illustrated by Fig. 9, which shows the measured wall superheating ΔT_{ONB} plotted versus the system pressure p at a constant degree of subcooling and for different mass fluxes.

The influence of local subcooling on wall superheating at the beginning of nucleate boiling can be seen in Fig. 10, which presents a plot of wall superheating ΔT_{ONB} versus the degree of subcooling for three different system pressures and varying mass fluxes.

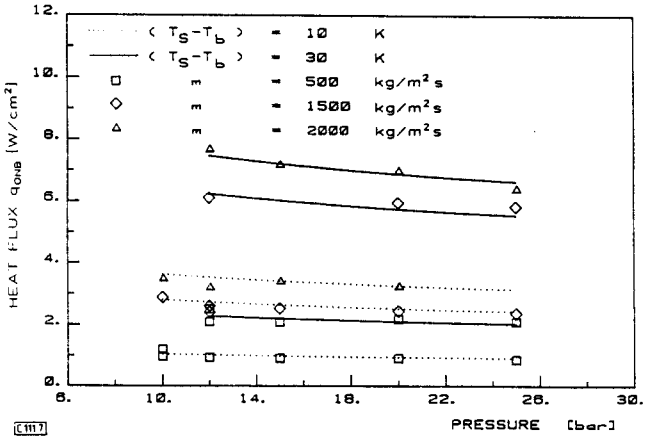

Fig. 7. Influence of system pressure on heat flux q_{ONB}.

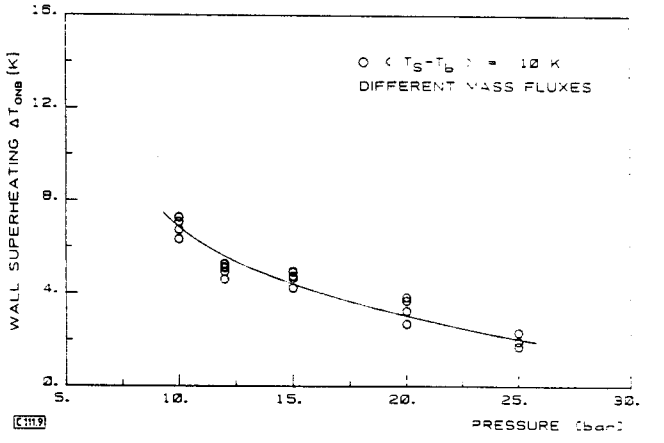

Fig. 9. Wall superheating as a function of pressure.

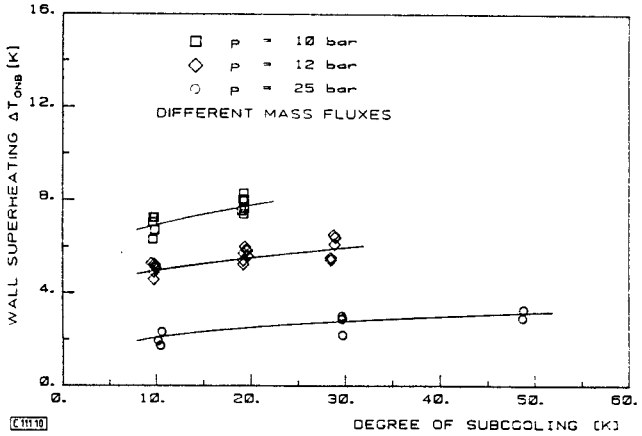

Fig. 10. Measured wall superheating versus degree of subcooling at onset of nucleate boiling (R 12).

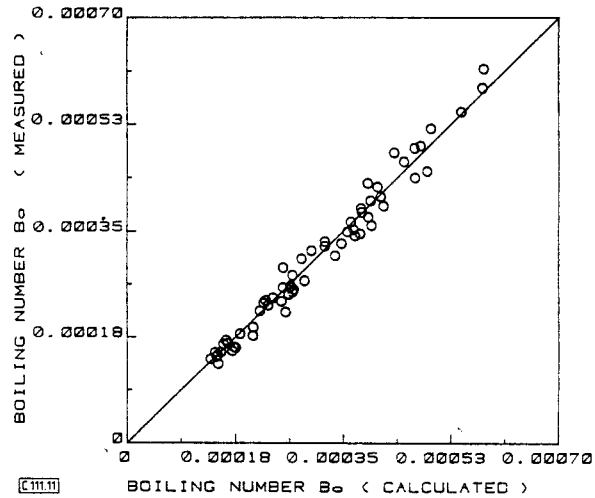

Fig. 11. Comparison of measured and calculated boiling numbers Bo(R12).

As is well known, the onset of nucleation is mainly affected by thermal and hydraulic conditions near the heated wall. In this region, variable subcooling of the bulk exerts only a slight influence on the physical properties. On the other hand, with increasing subcooling, the velocity gradient near the heated wall will decrease. Thus, the turbulent energy and turbulent thermal conductivity will also decrease which leads to an increase of wall superheating with increasing degree of subcooling, as shown in Fig. 10.

5 Regression Analysis

In order to formulate an equation for calculating the onset of nucleate boiling as a function of thermal and hydrodynamic parameters used in the present experiments, an empirical exponential equation of the following type was chosen:

$$\mathrm{Bo} = C\,\mathrm{Re}^{a}\left(\frac{p}{p_{\mathrm{crit}}}\right)^{b}\mathrm{Ja}_{\mathrm{mod}}^{c} \quad . \tag{4}$$

The Bo-number

$$\mathrm{Bo} = \frac{q_{\mathrm{onb}}}{m\,\Delta h_{\mathrm{v}}} \tag{5}$$

in Eq. (4) includes two parameters of main influence, namely the heat flux and the mass flux, whereas the Re-number

$$\mathrm{Re} = \frac{m\,D_{\mathrm{h}}}{\mu} \tag{6}$$

reflects the influence of the velocity profile.

Furthermore, the reduced pressure (p/p_{crit}) is used as a scaling parameter for modelling the thermodynamic parameters of different fluids.

The variable degree of subcooling is taken into account in the modified Ja-number

$$\mathrm{Ja}_{\mathrm{mod}} = \frac{h_{\mathrm{s}} - h_{\mathrm{inlet}}}{\Delta h_{\mathrm{v}}}\,\frac{\varrho_{\mathrm{l}} - \varrho_{\mathrm{g}}}{\varrho_{\mathrm{g}}} \quad . \tag{7}$$

To determine constant C and exponents in Eq. (4), a stepwise multiple regression analysis was employed. The result of this calculation is summarized in Eq. (8).

$$\mathrm{Bo} = 0.0015\,\mathrm{Re}^{-0.112}\,\frac{p}{p_{\mathrm{crit}}}\,\mathrm{Ja}_{\mathrm{mod}}^{0.773} \quad . \tag{8}$$

In the first consideration, it is astonishing that the exponent on the Re-number in Eq. (8) is negative and, as a result, the mass flow rate also has a negative exponent. Taking into account the fact that the mass flux is included in the denominator of the Bo-number as well, the resultant exponent on the mass flux will be 0.89 and this value is in good agreement with the correlations from literature for single-phase flow.

A comparison between the measured Bo-number and that calculated by Eq. (8) is presented in Fig. 11. It is seen that the results of the present experiments are reproduced by Eq. (8) with a mean deviation of ± 7%.

In order to illustrate the whole range of the selected modified Jacob number, Fig. 12 shows the term $\mathrm{Bo}/\mathrm{Re}^{-0.112} * (p/p_{\mathrm{crit}})$ plotted against the modified Ja-number. The experimental data are well approximated by a straight line.

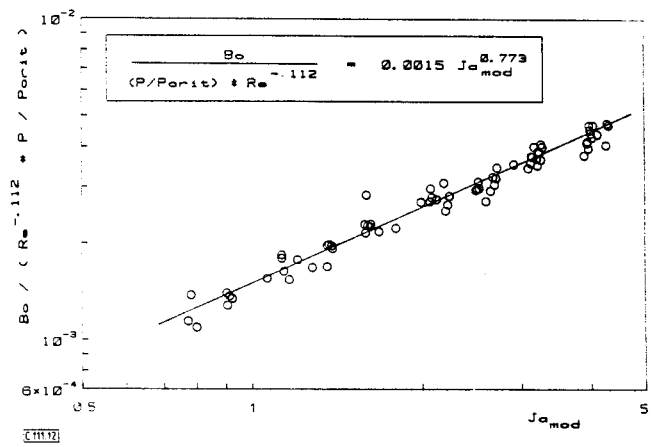

Fig. 12. Onset of nucleate boiling of R 12 in a dimensionless representation.

5.1 Comparison of Analytical Prediction with Water Data

In order also to check how Eq. (8) predicts the water data, the thermodynamic state and dimensionless numbers in Eq. (8) were scaled as follows:

$$p/p_{crit}\ (R\ 12) = p/p_{crit}\ (H_2O)\ ,$$

$$Ja_{mod}\ (R\ 12) = Ja_{mod}\ (H_2O)\ ,$$

$$Re\ (R\ 12) = Re\ (H_2O).$$

Using the calculation procedure, explained in chapter 3, the radial temperature profiles can be evaluated, taking into account Eq. (8) both for R 12 and water. The obtained results are illustrated in Fig. 13 which shows the temperature ratios $(T-T_S)\ /\ (T_S-T_i)$ plotted versus the radial distance from the heated wall.

It is obvious that the temperature gradient near the heated wall, expressed as the difference between the fluid temperature T and the saturation temperature T_S, based on the radial distance Δr, will be lower in the case of water. In view of the scaling procedure, this indicates that the wall superheating $(T_W - T_S)$ of water will be smaller than that of R 12 at the onset of nucleate boiling.

A comparison between the data calculated with the derived correlation for water and the experimental ones from [14] for the onset of nucleate boiling in water is shown in Fig. 14 which presents the heat flux q_{ONB} plotted versus the local subcooling for two different mass fluxes at constant pressure.

It can be seen that Eq. (8) yields a satisfactory prediction of the heat flux at the onset of nucleate boiling in water over the whole range of local subcooling.

Following conclusions were drawn from the results:

- In the case of R 12, a large deviation from thermodynamic equilibrium is observed prior to nucleation. The superheating is abruptly reduced following nucleation. As a result, a forced convection boiling curve is obtained with very pronounced hysteresis.
- The large wall superheating at incipient boiling can be explained by deactivation (flooding) of larger nucleation sites through a thorough wetting by R 12 and is also caused by the difference in physical properties between the refrigerant and water.
- A dimensionless equation for the onset of nucleate boiling was derived by regression analysis. This equation represents the authors' experimental data very well and, in the investigated parameter range, is also valid for water.

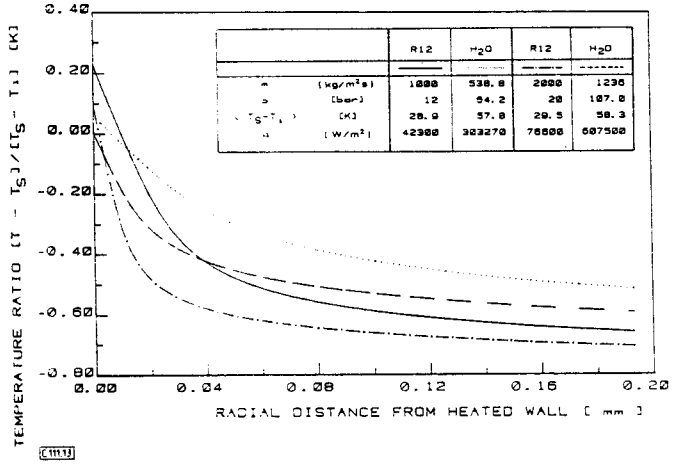

Fig. 13. Comparison of radial temperature ratios R 12 – H_2O.

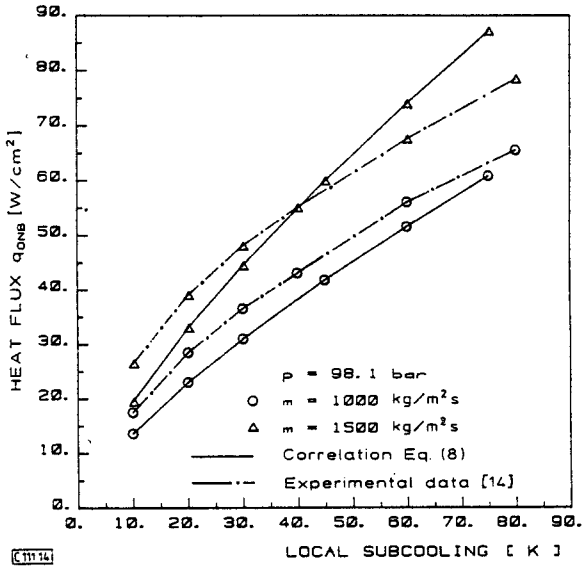

Fig. 14. Comparison of calculated and experimental data for onset of nucleate boiling in water.

Received: January 12, 1988 [CET 111]

Symbols used

A	[m²]	area
Bo	[–]	Boiling number
c	[J/kg K]	specific heat capacity
d, D	[m]	diameter
Δh	[J/kg]	latent heat of evaporation
i.d.	[m]	inner diameter
Ja	[–]	Jacob number
k	[W/m K]	thermal conductivity
k	[J/kg]	turbulent energy
L	[m]	length
m	[kg/m² s]	mass flux
o.d.	[m]	outer diameter
p	[bar]	system pressure
q	[W/m²]	heat flux
r,R	[m]	radius
Δr	[m]	radial coordinate difference
Re	[–]	Reynolds number
T	[°C, K]	temperature
ΔT	[K]	temperature difference
u	[m/s]	velocity
x	[m]	axial length
Δx	[m]	axial coordinate difference

Greek symbols

μ	[kg/m s]	viscosity
ϱ	[kg/ m^3]	density
σ	[N/m]	surface tension
ε	[m^2/s^3]	dissipation rate of turbulence

Subscripts

b	bulk fluid property
crit	critical
eff	effective
fc	forced convection
fric	friction
g	gas
h	hydraulic
i, inlet	inner, inlet
l	liquid
mod	modified
o	outer
ONB	onset of nucleate boiling
p	constant pressure
sat, s	saturation value
t	turbulent
w	wall

References

[1] Sato, T., Matsumura, H., *Bull. Jpn. Soc. Mech. Eng. 7* (1964) pp. 392 – 398.

[2] Bergles, A.E., Rohsenow, W.M., *Trans. ASME, Ser. C 86* (1964) pp. 365 – 372.

[3] Davis, E.J., Anderson, G.H., *AIChE J. 12* (1966) pp. 774 – 780.

[4] Levy, S., *Int. J. Heat Mass Transfer 10* (1967) pp. 951 – 965.

[5] Staub, F.W., *Trans. ASME, Ser. C 90* (1968) pp. 151 – 157.

[6] Saha, O., Zuber, N., *Point of net vapour generation and vapour void fraction in subcooled boiling*, Proc. 5th Int. Heat Transfer Conf., Tokyo 4, 1974, pp. 175 – 179.

[7] Bjorge, R.W., Hall, G.R., Rohsenow, W.M., *Int. J. Heat Mass Transfer 25* (1982) No. 6, pp. 753 – 757.

[8] Sekoguchi, K., Nishikawa, K., Nakasatomi, M., Hirata, N., Higuchi, H., *Flow boiling in subcooled and low quality regions – heat transfer and local void fraction*, Proc. 5th Int. Heat Transfer Conf., Tokyo 4, 1974, pp. 180 – 184.

[9] Hino, R., Ueda, T., *Int. J. Multiphase Flow 11*, (1985) No. 3, pp. 269 – 281.

[10] Abdelmessih, A.H., Fakhri, A., Yin. S.T., *Hysteresis effects in incipient boiling superheat of freon 11*, Proc. 5th Int. Heat Transfer Conf., Tokyo 4, 1974, pp. 165 – 169.

[11] Butterworth, D., Shock, R.A., *Flow boiling*, Proc. 7th Int. Heat Transfer Conf., Munich 1, 1982, pp. 11 – 30.

[12] Norris, L.H., Reynolds, W.C., *Channel Flow with a Moving Wavy Boundary*, Report No. FM-10, Stanford Univ. Dept. Mech. Eng, Stanford 1975.

[13] Mayinger, F., *Strömung und Wärmeübergang in Gas-Flüssigkeits-Gemischen*, Springer-Verlag, Wien, New York, 1982.

[14] Hein, D., Köhler, W., *Messungen zum Siedebeginn in hochbelasteten Kanälen*, Report Nr. 43.02.05, MAN, 1969.

Modelling of Multiphase Detonations with Drop Disintegration – Description of Thermal Detonations

Constantinos Carachalios, Hermann Unger and Manfred Bürger*

A model is presented which consists of steady-state and transient codes for the description of reacting multiphase flow fields, including hydrodynamic fragmentation of liquid drops in relative flows. An application of this model for the description of large scale melt-coolant interactions (thermal detonations) is described. A simulation of two-phase chemical detonations, especially those with hydrodynamic disintegration of liquid fuel drops in the reaction zone, is possible, in principle, within the framework of the modelling.

1 Introduction

Two-phase detonation phenomena have been investigated in the past not only in relation to many industrial applications, especially with the emphasis on optimization of combustion engines, but also with respect to safety (see e.g. [1, 2]). A special type of a two-phase explosive event is the so-called "vapour explosion", which can take place when a hot melt interacts with a volatile coolant. This phenomenon has been investigated mainly in relation to the safety of nuclear reactors (see e.g. [3, 4]).

The key phenomenon to be described in the modelling of thermal detonations is the fragmentation of melt drops within the detonation wave and the corresponding release of their thermal

* Dr. C. Carachalios, Europäisches Patentamt, D-8000 München, Prof. Dr.-Ing. H. Unger, Lehrst. für Nukleare und Neue Energiesysteme, Ruhr-Universität Bochum, Universitätsstr. 150, D-4630 Bochum, and D.P. M. Bürger, Inst. für Kernenergetik und Energiesysteme, Univ. Stuttgart, Pfaffenwaldring 31, D-7000 Stuttgart 80.

© VCH Verlagsgesellschaft mbH, D-6940 Weinheim, 1988

0930-7516/88/0510-0327 $02.50/0